RESEARCH ARTICLE | JULY 31 2023

Robust relativistic many-body Green's function based approaches for assessing core ionized and excited states

Max Kehry ; Wim Klopper ; Christof Holzer ✉

Check for updates

View Online   Export Citation   CrossMark

Articles You May Be Interested In

Focusing x-ray spectrograph with crossed dispersion

Rev Sci Instrum (March 2003)

Application of the focusing x-ray spectrograph with crossed dispersion to investigations of X pinch plasmas

Rev Sci Instrum (October 2004)

15 August 2023 15:25:26

Robust relativistic many-body Green's function based approaches for assessing core ionized and excited states

View Online   Export Citation   CrossMark

Max Kehry,[1,a] (iD) Wim Klopper,[1,b] (iD) and Christof Holzer[2,c] (iD)

AFFILIATIONS

[1] Institute of Physical Chemistry, Karlsruhe Institute of Technology (KIT), Fritz-Haber-Weg 2, 76131 Karlsruhe, Germany

[2] Institute of Theoretical Solid State Physics, Karlsruhe Institute of Technology (KIT), Wolfgang-Gaede-Straße 1, 76131 Karlsruhe, Germany

[a] Electronic mail: max.kehry@partner.kit.edu
[b] Electronic mail: klopper@kit.edu
[c] Author to whom correspondence should be addressed: christof.holzer@kit.edu

ABSTRACT

A two-component contour deformation (CD) based *GW* method that employs frequency sampling to drastically reduce the computational effort when assessing quasiparticle states far away from the Fermi level is outlined. Compared to the canonical CD-*GW* method, computational scaling is reduced by an order of magnitude without sacrificing accuracy. This allows for an efficient calculation of core ionization energies. The improved computational efficiency is used to provide benchmarks for core ionized states, comparing the performance of 15 density functional approximations as Kohn–Sham starting points for *GW* calculations on a set of 65 core ionization energies of 32 small molecules. Contrary to valence states, *GW* calculations on core states prefer functionals with only a moderate amount of Hartree–Fock exchange. Moreover, modern *ab initio* local hybrid functionals are also shown to provide excellent generalized Kohn–Sham references for core *GW* calculations. Furthermore, the core–valence separated Bethe–Salpeter equation (CVS-BSE) is outlined. CVS-BSE is a convenient tool to probe core excited states. The latter is tested on a set of 40 core excitations of eight small inorganic molecules. Results from the CVS-BSE method for excitation energies and the corresponding absorption cross sections are found to be in excellent agreement with those of reference damped response BSE calculations.

I. INTRODUCTION

The *GW* method has become a staple to assess the valence and core excited states of complex molecular systems, being a helpful theoretical tool for the well established fields of UV/Vis and x-ray spectroscopy. The latter is an especially valuable tool in the characterization of complex materials. The usage of high-energy radiation allows for the direct excitation of electrons occupying states close to the nuclei. Since the core energy states are highly element specific, x-ray spectroscopy can be employed to obtain information about the local (electronic) structure of a system. For example, it allows one to gain new insights into complex bonding situations in lanthanoid containing molecular systems.[1] Likewise, the description of these experiments using quantum mechanical methods is complicated and remains an active field of development, as the high-energy regime represents a difficult case, where small errors may be largely amplified.

While time-dependent density functional theory (TD-DFT) often provides a reasonable description, its applications to the x-ray regime regularly require the introduction of large energetic shifts,[2,3] which partly arise from the amplification of the self-interaction error in density functional approximations (DFAs).[4–8] Similarly, the ambiguity in the choice of the DFA needs to be studied carefully.[2,9,10] Contrary, wave function-based methods require a significant computational effort in order to systematically improve upon the more commonly employed DFT based approaches. Therefore, wavefunction based methods that are able to assess core excited states are limited to systems with only a few light atoms. Alternatives to

TD-DFT and wavefunction based methods to assess core excited states with high accuracy are, therefore, needed to gain insights into the light–matter interactions of core states of more complex molecular systems. In a recent article, we combined the damped response formalism with the Bethe–Salpeter equation (BSE) or, more specifically, the composite GW-BSE approach. In the GW-BSE approach, first the quasiparticle energies are obtained from the GW method. In the second step, charge-neutral excited states are obtained from the BSE, which is solved in the static screened approximation.[2] While the initial study was limited to the description of small molecules and atoms at the one- and two-component levels, that is, including scalar relativistic effects and spin–orbit coupling (SOC), it could be shown that the GW-BSE method is a powerful tool to assess core excited states. A scalar-relativistic study carried out by Yao and co-workers later came to similar conclusions.[11] Both studies indicated that the GW-BSE method provides a reasonable alternative to other established techniques, especially with respect to experimental reference results, thereby largely eliminating the need for an artificial shift of the spectrum as needed in TD-DFT.[2,11,12] The computational scaling of the BSE is likewise the same as for TD-DFT, making it even more interesting in the framework of core excitations. Still, a straightforward application of the GW-BSE method to more realistic systems, that is, systems with more than a few atoms, provides additional challenges to the method. This is especially true if relativistic effects as, for example, spin–orbit coupling are taken into account.[13–15] Here, the calculation of the quasiparticle energies from the GW method may quickly become a bottleneck. On one hand, common techniques, such as the contour deformation (CD) approach introduced in the 1980s, scale unfavorably if low-lying states, such as core orbitals, are of concern.[16–18] On the other hand, the analytic continuation of the GW self-energy yields significantly deteriorated quasiparticle energies for core states.[12]

The aim of the manuscript is twofold. First, we introduce a more pragmatic yet accurate approximation to the GW method for the calculation of the quasiparticle energies for core states in one- and two-component frameworks, based on the work of Duchemin and Blase.[19] This work is then combined with reduced scaling GW algorithms,[12,19–28] with a special focus on current relativistic implementations.[14,15] Given the high interest in open-shell relativistic systems, such as many lanthanoid containing systems, we will furthermore expand our method toward them. The GKS determinants of systems with unpaired electrons usually do not exhibit Kramers symmetry and are, therefore, especially challenging for TD-DFT and the GW-BSE method.[29] Contour deformation based GW could, however, recently be extended to such systems, allowing us to step forward in this direction.[15] The resulting strictly $\mathcal{O}(N^4)$ scaling relativistic frequency-sampled contour deformation GW (fsCD-GW) algorithm is able to efficiently assess quasiparticle states far away from the Fermi level, yielding core ionization energies with high accuracy. Furthermore, we hope that the fsCD-GW method will provide an entry point for even lower scaling GW algorithms.[30–35] fsCD-GW is finally combined with the BSE in the core–valence separation (CVS) approximation. The latter projects out, that is, freezes, valence orbitals, or spinors, to directly access core excited states, while including their screening effects in the dielectric matrix. Subsequently, we apply the resulting fsCD-GW method as well as the CVS-BSE method to sets of small organic

and inorganic molecules and compare the results to experimentally obtained values.

II. EFFICIENT QUASIPARTICLE ENERGIES FOR CORE STATES

The quasiparticle (QP) energies, ε^{QP}, are directly related to the charge excitations of a system and thereby useful for the estimation of electron affinities, ionization energies, or may act as an important ingredient in the calculation of charge-neutral excitations in the composite GW-BSE method. Quasiparticle energies can be obtained from the eigenvalues of a suitable reference system, here given by the generalized Kohn–Sham (GKS) system, with ε^{GKS} being the GKS eigenvalues, according to

$$\varepsilon_p^{QP} = \varepsilon_p^{GKS} + Z_p \langle p^{GKS}|\mathscr{R}[\Sigma(\varepsilon_p^{QP})] - v^{xc}|p^{GKS}\rangle, \quad (1)$$

where the exchange-correlation potential, v^{xc}, is substituted by the real part of the self-energy, Σ. The imaginary part of the self-energy Σ is related to the lifetime of the quasiparticle state. Z_p is a linearization or renormalization parameter that can be derived from the Taylor expansion of the quasiparticle equation around the respective GKS eigenvalue.[36] It is also related to the weight of a specific solution, given the non-linear structure of the QP equation, allowing for multiple solutions to the above equation.[36] Note that only the diagonal elements of $\Sigma(\varepsilon_p^{QP})$ are considered in the following, as they usually recover the major correction to the reference eigenvalues. The resulting single-shot G_0W_0 and eigenvalue self-consistent evGW methods are commonly used in order to obtain sufficiently accurate approximate QP energies.[37] Although a self-consistent solution would be independent of the initial starting point when updating also off-diagonal elements, the necessary computational cost quickly becomes prohibitive for relativistic systems. Fully self-consistent GW is, therefore, not discussed in this work. Furthermore, in the following sections, the indices $i, j, k, \ldots, (a, b, c, \ldots)$ denote occupied (virtual) spinors, $p, q, r, \ldots$ denote general spinors, and upper case indices $P, Q, R, \ldots$ will denote auxiliary basis functions.

According to Hedin, the self-energy in the GW approximation is given by[38]

$$\Sigma(\boldsymbol{x}, \boldsymbol{x}'; \omega) = \frac{i}{2\pi} \int_{-\infty}^{\infty} G(\boldsymbol{x}, \boldsymbol{x}'; \omega + \omega') W(\boldsymbol{x}, \boldsymbol{x}'; \omega') e^{i\omega'0^+} d\omega', \quad (2)$$

where G is the one-particle Green's function,

$$G(\boldsymbol{x}, \boldsymbol{x}'; \omega) = \sum_q \frac{\phi_q(\boldsymbol{x})\phi_q^*(\boldsymbol{x}')}{\omega - \varepsilon_q + i\eta \, \mathrm{sgn}(\varepsilon_q - \varepsilon^F)}, \quad (3)$$

and W is the screened exchange,

$$W(\boldsymbol{x}, \boldsymbol{x}'; \omega) = \int \kappa^{-1}(\boldsymbol{x}, \boldsymbol{x}''; \omega) v(\boldsymbol{x}'', \boldsymbol{x}') d\boldsymbol{x}'', \quad (4)$$

with ε^F being the energy of the Fermi-level, κ being the dielectric function, and v being the Coulomb interaction. η is a regularization parameter and is chosen as $\eta \to 0^+$ to keep all terms finite.

For convenience, the self-energy Σ can be split into the exchange and dynamic correlation contributions, Σ^x and Σ^c, respectively,

$$\Sigma(\boldsymbol{x}, \boldsymbol{x}'; \omega) = \Sigma^x(\boldsymbol{x}, \boldsymbol{x}'; \omega) + \Sigma^c(\boldsymbol{x}, \boldsymbol{x}'; \omega), \quad (5)$$

$$\Sigma^x(\boldsymbol{x}, \boldsymbol{x}'; \omega) = \frac{i}{2\pi} \int_{-\infty}^{\infty} G(\omega + \omega') v(\boldsymbol{x}, \boldsymbol{x}') e^{i0^+ \omega'} \, d\omega', \qquad (6)$$

$$\Sigma^c(\boldsymbol{x}, \boldsymbol{x}'; \omega) = \frac{i}{2\pi} \int_{-\infty}^{\infty} G(\omega + \omega') \underbrace{W^c(\boldsymbol{x}, \boldsymbol{x}'; \omega')}_{(W-v)} e^{i0^+ \omega'} \, d\omega'. \qquad (7)$$

Equation (6) refers to a static Fock-like exchange term, which is readily available in most quantum mechanical software packages and can be efficiently evaluated. Contrary, the second term of Eq. (5) requires further consideration. Note that it does include static contributions, as it does not vanish in the limit of $\omega \to 0$. This limit is just the Coulomb hole plus screened exchange or COHSEX approximation.[39] W^c is used to refer to the correlation part of the screened interaction. In the above expressions, the direct random-phase approximation (RPA) was invoked, in order to avoid the explicit calculation of the full vertex function. We, therefore, replace the fully interacting response of the systems, χ, with the non-interacting response function, χ_0, in the calculation of the dielectric function κ. The latter can be calculated within the RPA as

$$\kappa = 1 - \chi_0 \mathbf{v}. \qquad (8)$$

While a fully analytic evaluation of the resulting expression is available via knowledge of the full spectral representation of the response function, the computational complexity of the spectral approach grows as $\mathcal{O}(N^6)$, where N is a measure of the size of the system considered. The associated cost of the spectral approach, therefore, quickly becomes prohibitively large.[36,40,41] If spin–orbit effects are to be considered, as in two-component (2c) or four-component (4c) formulations, the accessible space of (chemically) relevant systems for many applications further decreases dramatically for the spectral approach.[14,42] Analytic continuation and contour deformation techniques are, however, viable alternatives that have shown to perform well in relativistic two-component GW calculations.[14,15,23]

A. Contour deformation technique in GW using auxiliary subspace methods

As Golze and co-workers pointed out, analytic continuation of the correlation part of the self-energy may often be unsuitable for the calculation of quasiparticle energies of states further away from the Fermi level, due to its complicated structure along the real axis.[12] Thus, alternative approaches based on contour deformation are usually better suited for core states and related problems. Employing the contour deformation technique,[14,18,43] the correlation part of the self-energy may be written as

$$\begin{aligned}
\Sigma^c(\omega) &= \frac{i}{2\pi} \oint G(\omega + \omega') W^c(\omega') \, d\omega' \\
&\quad - \frac{1}{2\pi} \int_{-\infty}^{\infty} G(\omega + i\omega') W^c(i\omega') \, d\omega', \\
&= R^c(\omega) + I^c(\omega), \qquad (9)
\end{aligned}$$

where $R^c(\omega)$ and $I^c(\omega)$ correspond to the contour integral and the integral along the imaginary axis, respectively. The contour integral

$R^c(\omega)$ can be simplified by employing the residue theorem, as discussed in earlier works.[12,14,18] For an arbitrary state p, the contour integral $R^c(\omega)$ reads

$$R^c_p(\omega) = \sum_q f_q(\omega) W^c_{pq,pq}(|\omega - \varepsilon_q| + i\eta). \qquad (10)$$

The prefactor $f_q(\omega)$ is given by

$$f_q(\omega) = \begin{cases} +1 & \text{if } \varepsilon^F \le \varepsilon_q < \omega, \\ -1 & \text{if } \varepsilon^F > \varepsilon_q > \omega, \\ +\dfrac{1}{2} & \text{if } \varepsilon^F \le \varepsilon_q = \omega, \\ -\dfrac{1}{2} & \text{if } \varepsilon^F > \varepsilon_q = \omega, \\ 0 & \text{else} \end{cases} \qquad (11)$$

and can be determined from the energetic location of the orbital or spinor with respect to the Fermi level ε^F. Note that $f_q(\omega)$ is defined in accordance with Ref. 14, where the cases with $\omega = \varepsilon_q$ are discussed specifically.

The integral along the imaginary axis can similarly be written as

$$I^c_p(\omega) = -\frac{1}{2\pi} \sum_q \int_{-\infty}^{\infty} \frac{W^c_{pq,pq}(i\omega') \, d\omega'}{\omega + i\omega' - \varepsilon_q + i\eta \operatorname{sgn}(\varepsilon_q - \varepsilon^F)}. \qquad (12)$$

Equation (12) can conveniently be evaluated using numerical quadrature schemes, for example, with Gauss–Legendre quadrature. While the integration along the imaginary axis in Eq. (12) is the time-determining step for valence states, it is constant and independent of the specific orbital or spinor for which the correlation part of the self-energy is to be calculated. The computational demand for the evaluation of the correlation part of the self-energy arising from Eq. (10), however, depends heavily on the state of interest. The gross number of the residuals in Eq. (10) needed for a given orbital or spinor scales directly with the number of states in between the state of interest and the Fermi level. Therefore, for the lowest lying $1s$ state, for example, the sum in Eq. (10) runs over all occupied states.

The matrix elements of the screened exchange W can be calculated as

$$W_{pq,rs}(\omega) = \sum_{tu} [\kappa(\omega)]^{-1}_{pq,tu} v_{tu,rs}, \qquad (13)$$

with $\kappa^{-1}_{pq,tu}(\omega)$ being the elements of the dielectric matrix as outlined in Eq. (8). Using the resolution-of-the-identity (RI) approximation, the Coulomb integrals can conveniently be expressed as

$$v_{pq,rs} \approx \sum_P B^{P*}_{pq} B^P_{rs}, \qquad (14)$$

where

$$B^P_{rs} = \sum_Q [V^{-1/2}]_{PQ} (Q|rs) \qquad (15)$$

is a three-index Coulomb integral. Furthermore, V^{-1} is the inverse of the Coulomb metric. The frequency-dependent polarizability $\Pi_{PQ}(\omega)$ within the RPA approximation can then be expressed as

$$\Pi_{PQ}(\omega) \approx \sum_{ai} \left[\frac{B_{ia}^P B_{ia}^{Q^*}}{\varepsilon_i - \varepsilon_a + \omega - i\eta} + \frac{B_{ai}^P B_{ai}^{Q^*}}{\varepsilon_i - \varepsilon_a - \omega + i\eta} \right]. \quad (16)$$

The above expression obeys certain symmetry relations on using the negative or complex conjugate frequencies ω. These relations can be exploited to lower the computational effort needed in the calculation of these quantities.[14,15] This is especially true for the case $\eta \to 0^+$, yielding purely real or imaginary frequencies ω. From the frequency-dependent polarizability $\Pi_{PQ}(\omega)$, the dielectric matrix is then obtained as

$$\kappa_{PQ}(\omega) = \delta_{PQ} + \Pi_{PQ}(\omega). \quad (17)$$

From the latter, the correlation part of the screened exchange $W^c(\omega)$ follows as

$$W_{pq,rs}^c(\omega) = \sum_{PQ} B_{pq}^{P^*} \left\{ \left[\kappa^{-1}(\omega) \right]_{PQ} - \delta_{PQ} \right\} B_{rs}^Q. \quad (18)$$

Inserting Eq. (18) into Eqs. (12) and (10) and subsequently Eq. (9) finally yields the correlation part of the self-energy.

B. Frequency sampled residue evaluation

While the calculation of the integral $I(\omega)$ scales as low as $\mathcal{O}(N^4)$ and is independent of the actual quasiparticle correction to be calculated, matters are different for $R(\omega)$. As outlined in Eqs. (10) and (11), for core orbitals, the sum over contributing states steadily grows with system size. Ultimately, for the lowest energy orbital, n_{occ} contributions are summed, each scaling as $\mathcal{O}(N^4)$, ultimately leading to a $n_{occ} \times \mathcal{O}(N^4) \approx \mathcal{O}(N^5)$ scaling behavior. Recently, Duchemin and Blase proposed a method in which the screened exchange is calculated for a series of frequencies, from which it is then analytically continued to the frequency of interest.[19] Using this method, Eq. (10) can be rewritten as

$$R_p^c(\omega) \approx \sum_m f_m(\omega) \widetilde{W}_{pm,pm}^c(|\omega - \varepsilon_m| + i\eta). \quad (19)$$

The correlation part of the screened exchange can then be represented by a rational function,

$$\widetilde{W}_{pm,pm}^c(z) = c_0 \left(1 + \frac{c_1(z - z_1)}{1 + \frac{c_2(z - z_2)}{1 + \cdots + c_N(z - z_n)}} \right)^{-1}, \quad (20)$$

where the coefficients c_N are implicitly dependent on the considered matrix element $W_{pm,pm}^c(z)$. Assuming the rational approximation can be used to adequately represent all required residues employing only a few reference frequencies z, the formal scaling of evaluating Eq. (10) is reduced to $\mathcal{O}(N^4)$. As outlined in Ref. 19, the advantage of analytically continuing the screened exchange instead of the self-energy lies in the much simpler structure of W. The latter only contains the poles associated with the charge-neutral excitations. The rational approximation is, therefore, assumed to be well-behaved, staying valid for larger frequency ranges.[19]

A simple choice of frequencies z, for which the dielectric function κ and subsequently W are evaluated, are the true

Gauss–Legendre roots used in Eq. (12). For the latter, W is readily available, causing no overhead in the algorithm. In order to stabilize the analytic continuation further, the imaginary frequency grid is extended by a set of reference points along the real axis.[19] Duchemin and Blase employed a set of additional supporting points, linearly spaced along the real axis, and shifted by η into the imaginary plane, where η was chosen between 0.1 and 1.5 eV.[19] In this work, we, instead, choose to use adaptive grids on the real axis as outlined in the following Sec. II C.

For the constructed list of reference points $z \in Z_s$, the corresponding correlation parts of the screened exchange are consecutively evaluated according to Eq. (18). Assuming the dielectric function to be well represented by a suitable rational approximation having a reference point in close proximity, a set of weights ω_j is fitted to the correlation part of the screened exchange by the means of the Adaptive Antoulas-Anderson (AAA) algorithm as[44,45]

$$W_{pm,pm}^c(z) = \frac{P(z)}{W(z)} = \frac{\sum_j^n \frac{w_j W_{pm,pm}(z)}{z - z_j}}{\sum_j^n \frac{w_j}{z - z_j}}. \quad (21)$$

The optimal weights for Eq. (21) can be found in a least-squares manner from a linear system of equations by minimizing the function,

$$\left| \sum_j^n \frac{w_j W_{pm,pm}(z)}{z - z_j} - \sum_j^n \frac{w_j W_{pm,pm}(z_j)}{z - z_j} \right|, \quad (22)$$

while requiring that

$$\sum_j |w_j|^2 = 1. \quad (23)$$

The resulting linear systems of equations can, for example, be solved using a singular value decomposition. In practice, the rational approximation is obtained in an iterative manner, where a new reference point is only included if the previous approximation was unable to provide a reasonable approximation to it, based on the largest deviation. Using the obtained set of weights w_j, $W_{pm,pm}^c(\omega)$ can finally be evaluated by re-inserting the weights and setting $z = \omega$ in Eq. (21). Since the approximation has poles at the reference points, frequencies within $5 \cdot 10^{-6}$ a.u. are directly approximated by the closest reference point. Within this threshold, variations in the dielectric function are neglected.

C. Construction of the reference grid for frequency sampling on the real axis

Frequencies used to evaluate Eqs. (10) and (11) often occur in close proximity, forming groups (or clusters), which can be related to the different atomic shells. The goal is to represent these groups by only a few (usually one) discrete frequencies. For a core state, the residues associated with valence electrons are, therefore, ideally represented by only a small amount of actual additional real frequencies. The resulting set of grid points on the real axis is then suitably sparse. To construct a suitable list of frequency grid points $z \in Z_s$ on the real axis, first, a list of all contributing frequency values according to Eqs. (10) and (11) are assembled. If occupied and unoccupied states are to be considered, the list of points is constructed to be symmetric with respect to the origin, requiring that if $z \in Z_s$ then also $-z \in Z_s$.

In the next step, frequencies z_j that are too similar to their nearest other frequency z_i are eliminated from the list altogether. Starting from the lowest frequency, usually $z_{i=1} = 0.0$ representing the case $\varepsilon_q = \omega$ in Eq. (11), a frequency $z_j > z_i$ is discarded if

$$|z_i - z_j| < T_1 \qquad (24)$$

or if

$$\frac{|z_i - z_j|}{\min(z_i, z_j)} < T_2. \qquad (25)$$

The threshold T_1 is set to 0.05 a.u. (1.36 eV), and the threshold T_2 is set to 0.001, respectively. This compare-and-discard step can be performed in an $\mathcal{O}(N \cdot \log N)$ manner with adequate sorting algorithms. The remaining real frequencies are added to the imaginary Gauss–Legendre roots used to evaluate Eq. (12) to form the full list of frequencies Z_s. Take note of the previously mentioned threshold of $5 \cdot 10^{-6}$ a.u., for which we assume the dielectric function to not vary significantly. This acts as a lower bound to T_1. Residues that fall into this threshold use the same dielectric function and are evaluated directly. Figure 1 shows the result of this real frequency sampling for the pyridine molecule and a Cd_{14} cluster. To obtain the correlation part of the self-energy of the 1s state, for the canonical CD-G_0W_0 approach, 21 and 672 residues need to be determined according to Eq. (11) for pyridine and Cd_{14}, respectively. Clustering of the corresponding residues allows the frequency sampling algorithm to reduce the number of frequency points to 9 (pyridine) and 7 (Cd_{14}) without any significant loss in accuracy of the obtained correlation part of the self-energy and subsequently the quasiparticle energy. Unlike the canonical CD-G_0W_0 algorithm, which is, for larger systems like the Cd_{14} cluster, dominated by the task of calculating Eq. (10) for all 672 residues, the fsCD-G_0W_0 algorithm is dominated by the evaluation of the numerical integral in Eq. (12). The latter is evaluated using 64–256 frequency points on a Gauss–Legendre grid and is independent of the actual investigated spinor.

We note, in passing, that while for time-reversal symmetry breaking GKS references $W^c(z) \neq W^c(-z)$, it is still sufficient to construct $\Pi_{PQ}(\omega)$ only for those points of Z_s with $\mathscr{R}(z) > 0$ and then exploit the known symmetry relations of $\Pi_{PQ}(\omega)$.[15] By constructing adaptive grids for individual systems, a balanced description is obtained for each system using a minimal number of actual frequencies, for which Eq. (16) needs to be evaluated.

III. ASSESSING CORE EXCITED STATES USING THE BETHE–SALPETER EQUATION

Core excitations or regions with a high spectral density are usually inaccessible using standard linear response solvers that extract each excitation separately, that is, in a pole-by-pole manner. For molecules with more than a few atoms, core excitations are buried deep in the optical response spectrum, with hundreds of thousands of excitations being energetically lower and, therefore, preferably extracted by standard solvers based on the Davidson algorithm or similar eigenvalue solvers. Accordingly, special strategies need to be employed to tackle core excitations. Similar things hold true for spectral dense regions, as, for example, occurring in metal clusters or plasmonic systems, where even the visible range is already occupied by tens of thousands of single excitations that compose the optical
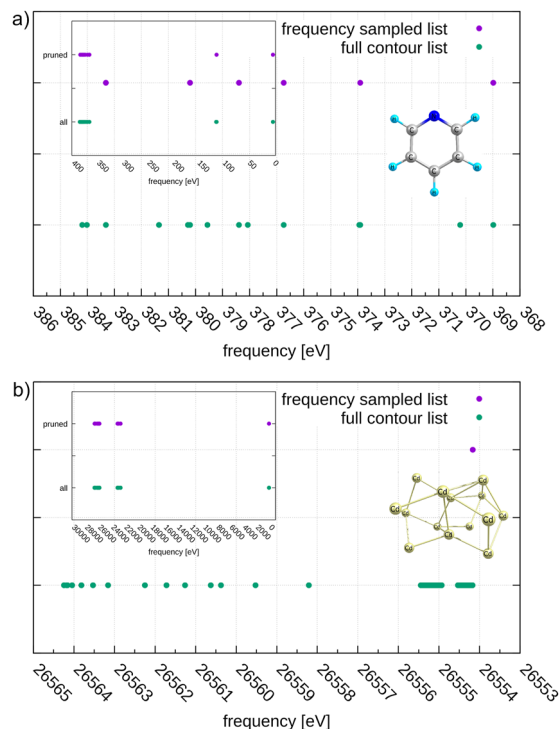

FIG. 1. Distribution of grid points of residues for (a) pyridine and (b) a Cd_{14} cluster obtained from Eq. (11) (green points) and frequencies obtained from the frequency sampling algorithm (purple dots) in the vicinity of the corresponding 1s orbitals. The inset shows the distribution over the whole frequency range. For pyridine, the 21 possible residues (green dots) are reduced to 9 frequencies (purple dots). For the Cd_{14} cluster, there are a total of 672 residues, while only 7 frequencies are sampled, outlining the strong clustering of the actual residues.

response. In these cases, pole-by-pole solvers become inefficient, and one has to resort to different techniques.

A. The core–valence separated Bethe–Salpeter equation

The first possibility to assess core excited states within the static-screened BSE is the core–valence separation (CVS) approximation.[46–49] Within the CVS, the BSE adopts the same structure as the corresponding adiabatic CVS-TD-DFT equations,[50,51]

$$\begin{pmatrix} \mathbf{A} & \mathbf{B} \\ -\mathbf{B}^* & -\mathbf{A}^* \end{pmatrix} \begin{pmatrix} \mathbf{X} & \mathbf{Y}^* \\ \mathbf{Y} & \mathbf{X}^* \end{pmatrix} = \begin{pmatrix} \mathbf{X} & \mathbf{Y}^* \\ \mathbf{Y} & \mathbf{X}^* \end{pmatrix} \begin{pmatrix} \Omega^+ & \mathbf{0} \\ \mathbf{0} & -\Omega^+ \end{pmatrix}, \qquad (26)$$

with the matrices $\mathbf{A}$ and $\mathbf{B}$ being defined as

$$A_{\bar{i}a,\bar{j}b} = (\varepsilon_a - \varepsilon_{\bar{i}})\delta_{ab}\delta_{\bar{i}\bar{j}} + \nu_{ia,bj} - K_{ab,\bar{i}\bar{j}} - W^c_{ab,\bar{i}\bar{j}}(\omega = 0), \qquad (27)$$

$$B_{\bar{i}a,\bar{j}b} = \nu_{ia,jb} - K_{ja,\bar{i}b} - W^c_{ja,\bar{i}b}(\omega = 0), \qquad (28)$$

where $K_{pr,rs}$ is the exact exchange, and $W^c_{pq,rs}(\omega = 0)$ is the correlation part of the screened exchange outlined in Eq. (18) at a frequency of zero. The occupied orbital space i, j is truncated in the CVS, as

noted by using the indices $\tilde{i}$ and $\tilde{j}$ in Eq. (26). This truncation allows us to effectively project out valence excitations, by removing valence spinors from the set of spinors encompassed by $\tilde{i}$ and $\tilde{j}$. Consequently, this enables a direct assessment of higher lying excitations. The excitation windows that should be investigated can, therefore, simply be set by the number of frozen valence orbitals. Note that for the construction of Π_{PQ} and consequently the dielectric function κ, which is needed to evaluate $W_{pq,rs}^c(\omega = 0)$, the full spinor space is used. The latter must not be truncated even if the spinor space of $W_{pq,rs}^c(\omega = 0)$ is truncated. The CVS has the appealing advantage that it still yields single excited states, and each can be analyzed in detail on its own. Furthermore, it utilizes the same solvers as GW-BSE,[14,52–55] so that only minor code modifications are necessary to implement the CVS approximation in program packages that already support solving standard BSE equations.

B. Damped response formalism for the Bethe–Salpeter equation

While the CVS approach is viable for accessing core excitations, it has two major drawbacks. First, it fully neglects the core–valence correlation. This drawback can, however, become a positive point, as neglecting core–valence correlation also removes spurious excitations from valence states to high-lying virtual orbitals. Second, the CVS-BSE may still be prohibitively expensive if the density of excited states is high, for example in metal clusters. The damped response can then provide a viable alternative to the CVS approach.[56,57] In the damped response formalism that has been outlined for the GW-BSE method by some of the authors in earlier publications,[2] the response to an external field is calculated directly as

$$\left[\begin{pmatrix} \mathbf{A} & \mathbf{B} \\ \mathbf{B}^* & \mathbf{A}^* \end{pmatrix} - (\omega + \mathrm{i}\Gamma) \begin{pmatrix} \mathbf{1} & 0 \\ 0 & -\mathbf{1} \end{pmatrix} \right] \begin{pmatrix} \mathbf{x} \\ \mathbf{y} \end{pmatrix} = \begin{pmatrix} \mathbf{p}^v \\ \mathbf{q}^v \end{pmatrix}. \quad (29)$$

$\mathbf{p}^v$ in Eq. (29) is a property vector, collecting the electric

$$p_{ia}^e = \langle \phi_i | \vec{r} | \phi_a \rangle \quad (30)$$

or magnetic

$$p_{ia}^m = \frac{1}{2c} \langle \phi_i | (\vec{r} - \vec{R}) \times \vec{\nabla} | \phi_a \rangle \quad (31)$$

dipole integrals, and $\mathbf{q}^v = (\mathbf{p}^v)^*$. Equation (29) can then be solved for a given set of frequencies $\omega_{ex} = (\omega + \mathrm{i}\Gamma)$, with ω and $\mathrm{i}\Gamma$ describing the real and imaginary frequencies of the external field. From the solution vector $\{\mathbf{x}(\omega_{ex}), \mathbf{y}(\omega_{ex})\}$, the frequency-dependent polarizability can then be obtained as

$$\alpha^{vv'}(\omega_{ex}) = \langle\langle \mathbf{x}^v(\omega_{ex}), \mathbf{y}^v(\omega_{ex}) | \mathbf{p}^{v'}, \mathbf{q}^{v'} \rangle\rangle. \quad (32)$$

In the damped response formalism, exact information about each discrete (single) excitation is lost. Instead, one directly extracts the polarizability as a function of the frequency, solving coupled perturbed BSE equations.[58,59] The main advantage of the damped response formalism is, therefore, that the spectral region of interest may be assessed without any restrictions on the number of excited states that are lower in energy. There is no need to extract the response of the visible region if one is interested in the core

region only. In contrast to the CVS approximation, furthermore, core–valence correlation is not neglected, as in $\mathbf{A}$ and $\mathbf{B}$ of Eq. (29), one may simply set $\tilde{i} = i$ and $\tilde{j} = j$. While this may re-introduce spurious excitations from valence to higher lying virtual orbitals, it may still be convenient to investigate the effects of core–valence correlation. Furthermore, it is possible to combine the CVS approximation with the damped response formalism, combining the best of both worlds if needed.

IV. COMPUTATIONAL METHODS

The fsCD-G_0W_0 and fsCD-evGW methods outlined in Sec. II B and CVS-BSE method outlined in Sec. III A were implemented in a locally modified version of Turbomole 7.7.[60,61] The implementation makes use of OpenMP parallelism as well as being capable of running on modern graphical processing units (GPUs).[62–64]

A. Validation of frequency-sampled contour deformation based GW

To validate the implementation and accuracy of the fsCD-GW approach, the 1s ionization energy as well as the HOMO ionization energy of the trivalent lanthanoids from Ce^{3+} to Yb^{3+} were investigated. The PBE0 functional was chosen, in combination with the all-electron relativistic x2c-QZVPPall-2c basis set. Suitable auxiliary basis functions have been used for the RI approximation.[65,66] The GW@PBE0/x2c-QZVPPall-2c method was shown to perform well for these ions,[15] and PBE0 is a broadly available density functional. Convergence thresholds of 10^{-9} hartree for the energy and 10^{-8} for changes in the atomic orbital density matrix were used. A grid of size 4 was used.[67] Calculations were done within a 2c formalism, including spin–orbit effects. Furthermore, a finite nucleus model was used.[68,69] For the evGW calculations, the spinors 55–80 were optimized in each iteration using (fs)CD-evGW, while the remaining spinors are being shifted accordingly ("scissoring"). Reference analytical results for the 1s spinors are obtained from the spectral $\mathcal{O}(N^6)$ representation using $\eta = 10^{-3}$.[70]

B. Scaling behavior of the frequency sampled contour deformation based GW algorithm

To test the scaling behavior of the fsCD-GW algorithm for core quasiparticle energies, the CD-G_0W_0@PBE0 and fsCD-G_0W_0@PBE0 quasiparticle energies of the 1s states are calculated for small cadmium clusters ranging from 4 to 18 atoms. The all-electron x2c-TZVPPall-2c basis set was used, in conjunction with a suitable auxiliary basis set.[65] Geometries of the cadmium clusters were taken from Ref. 71. All timings were measured on an Intel E5-2687W CPU, using eight threads. Kramers symmetry was exploited in 2c calculations.

C. Core-electron ionization energies from the CORE65 set from the GW method

To validate the different fsCD-GW approaches themselves, the core ionization energies of the CORE65 test set were evaluated.[72] This set is composed of core ionization energies associated with 30 C, 21 O, 11 N, and 3 F 1 s states for a set of 32 small organic and inorganic molecules. For all molecules, core ionization energies were calculated from the fsCD-G_0W_0@DFT and the

fsCD-evGW@DFT methods. All occupied states and the 20 lowest lying virtual states were optimized in the evGW treatment. The quasiparticle energies were evaluated for various density functional approximations. Specifically, they were evaluated for the pure DFAs BP86,[73,74] PBE,[75] TPSS,[76] and r^{2}SCAN,[77,78] the hybrid functionals B3LYP, BH & HLYP,[74,79,80] PBE0,[75,81] and TPSSh,[76,82] the range-separated hybrid functionals CAM-B3LYP,[83] ωB97X-D,[84] and LC-ωPBE,[85] and the local hybrid functionals Lh12ct-SsirPW92,[86] Lh14t-calPBE,[87] Lh20 t,[88] and TMHF.[89] The triple-ζ x2c-TZVPPall-2c and quadruple-ζ x2c-QZVPPall-2c basis sets were used, respectively, in combination with a suitable auxiliary basis set.[65,66] Convergence thresholds of 10^{-9} hartree for the energy and 10^{-8} for changes in the density matrix were used. A grid of size 4 was used for pure, hybrid, and range-separated hybrid functionals,[67] while an ultrafine grid was used for local hybrid functionals.[62] As only 1s states are investigated, spin–orbit effects are estimated to not be too important, and therefore, the spin-separated scalar relativistic exact two-component approach (X2C) is used. The finite nucleus model was used in all calculations. Note that unlike in Ref. 72, we do not add further corrections to the quasiparticle energies, as our model accounts for the most significant relativistic effects already. To assess the statistical error of each DFA, we use the same geometries and reference ionization energies as in Ref. 72.

D. K- and L-edges of small inorganic molecules from the core–valence separated GW-BSE method

To assess the performance of the CVS-GW-BSE approach, 40 core excited states of eight molecules associated with edges of the central metal (or metalloid) atoms, namely the L-edges of CrO_2Cl_2,[90] the L-edges of $VOCl_3$,[90] the K and L-edges of $PdCl_2$,[91] the K and L-edges of $SiCl_4$,[92] the K[93] and L-edges[94] of $FeCp_2$, and the K[95] and L-edges[96] of $TiCl_4$, $TiCl_3Cp$, and $TiCl_2Cp_2$, were investigated and compared to the respective experimental values. Convergence thresholds of 10^{-9} hartree for the energy and 10^{-8} for changes in the density matrix were used. A grid of size 5 was used for pure, hybrid, and range-separated hybrid DFAs,[67] while an ultrafine grid was used for local hybrid functionals.[62] For the CVS approximation, all non-core spinors with an energy higher than the spinor of interest were frozen and projected out. A 2c formalism was used, including spin–orbit effects through the full X2C Hamiltonian. A finite nucleus model was used, and SOC corrections to two-electron integrals were estimated using the modified screened nuclear spin–orbit (mSNSO) approach.[97–99] As including spin–orbit effects via the 2c formalism, using spinors instead of orbitals, adds significant computational strain, we limit the investigation of this set of molecules to the G_0W_0-CVS-BSE@DFT and evGW-CVS-BSE@DFT levels of theory. The triple-ζ x2c-TZVPPall-2c basis set was used, in combination with a suitable auxiliary basis set.[65,66] The PBE0 and TMHF functionals were chosen as a suitable basis for testing, as PBE0 is again broadly available and performs reasonably well, while TMHF was found to be an excellent performer for the CORE65 test set, yet with currently limited availability. Finally, damped response BSE is used to get a grasp of the accuracy of the CVS approximation. For this purpose, we calculate the core excitation spectra in the energy range of the well separated L-edges of CrO_2Cl_2, $VOCl_3$, $PdCl_2$, and $TiCl_3Cp$ using damped response BSE as outlined in Sec. III B and compare the obtained results with those from the CVS-BSE method.

V. RESULTS AND DISCUSSION

A. Validation of frequency-sampled contour deformation based GW

To validate the frequency-sampled contour deformation based GW algorithm outlined in Sec. II B, the self-energies of the 1s orbital of open-shell lanthanoids are investigated. The corresponding correlation parts of the self-energies are listed in Table I.

As outlined in Table I, fsCD-G_0W_0 nearly perfectly mimics the results obtained from canonical CD-G_0W_0. Both also perfectly align with the analytical $\mathcal{O}(N^6)$ results obtained from the spectral representation.[70] Notable deviations are only observed for the 1s spinor of Nd^{3+}, with (fs)CD-GW deviating by 0.02–0.04 eV from the analytical $\mathcal{O}(N^6)$. This amounts to a deviation of 0.005%–0.009% of the total correlation part of the self-energy for the 1s spinors. For Nd^{3+}, furthermore, the correlation part of the self-energy is rather large, especially when compared to the values found for the other lanthanoid ions. This is caused by a singularity being located in the vicinity of the quasiparticle peak. The latter leads to a rather steep slope of the correlation part in the region of interest and also to a stronger than usual dependence of the reference results on the chosen parameter η. A corresponding figure outlining this issue and further discussions of this case can be found in the supplementary material. Overall, fsCD-GW is in near perfect agreement with canonical CD-GW,[14,15] and both are in excellent agreement with spectral $\mathcal{O}(N^6)$ GW.[70] As time-reversal symmetry breaking GKS determinants correspond to the most challenging cases, it can safely be assumed that this excellent agreement will also be achieved for simpler non- and scalar-relativistic determinants. Furthermore, 2c and 4c GKS determinants that obey time-reversal symmetry are simply special cases of non-time reversal symmetric determinants in the framework of the corresponding fsCD-GW equations, and therefore, performance will be similar.

TABLE I. Correlation part of the self-energy (Σ^c) of the 1s orbital of the open shell lanthanoid ions Ce^{3+} to Yb^{3+}, calculated at the GW@PBE0 level of theory using canonical and frequency sampled (fs) contour deformation (CD) GW. All values in eV.

Ion	CD-G_0W_0	fsCD-G_0W_0	Full G_0W_0
Ce^{3+}	75.482	75.482	75.482
Pr^{3+}	77.514	77.514	77.514
Nd^{3+}	415.756	415.700	415.718[a]
Pm^{3+}	77.153	77.153	77.153
Sm^{3+}	78.976	78.976	78.976
Eu^{3+}	80.346	80.346	80.346
Gd^{3+}	81.626	81.626	81.626
Tb^{3+}	82.984	82.984	82.984
Dy^{3+}	84.319	84.319	84.319
Ho^{3+}	85.629	85.629	85.629
Er^{3+}	86.921	86.921	86.921
Tm^{3+}	88.209	88.209	88.209
Yb^{3+}	89.576	89.576	89.576

[a] A result of 415.756 eV is obtained with $\eta = 10^{-6}$.

For valence ionization potentials of trivalent lanthanoid ions, which have been shown to be rather accurate when evGW@PBE0 is used,[15] our findings are similar. Deviations of fsCD-evGW from CD-evGW are insignificant even when iteratively updating the quasiparticle energies as outlined in Table II. The only deviation being larger than 1 meV is found for Ce^{3+}, with a deviation of 5 meV when compared to the CD-evGW reference. This is remarkable, as 16 spinors are updated in each iteration, outlining that the deviation of the correlation part of the self-energy from fsCD-GW is vanishing when compared to the reference canonical CD-GW implementation. The frequency sampling algorithm does an excellent job, providing basically the same accuracy as the canonical algorithm at a significantly reduced cost. This is further outlined for the 1s orbital of the water molecule in the supplementary material, for which fsCD-G_0W_0 recovers the behavior of the correlation part of the self-energy for a broad frequency range around the point of interest.

B. Scaling behavior of the frequency sampled contour deformation based GW algorithm

After having shown the validity of the fsCD-GW approach, we turn to investigate the improved scaling behavior of this algorithm. Figure 2 outlines the computational time needed to perform scalar relativistic (1c) and relativistic (2c) (fs)CD-G_0W_0 calculations on a set of cadmium clusters with 4–18 atoms. Only the 1s spinors were optimized, and the corresponding timings are outlined in Fig. 2. Two important conclusions can be drawn from Fig. 2. First, the overall scaling of fsCD-GW is vastly improved, with the algorithm being nearly an order of magnitude faster than the canonical algorithm. This behavior is observed for both references, 1c and 2c, with the latter being approximately eight times more expensive to calculate initially but then exhibiting basically the same scaling behavior. Second, there is no crossover between frequency sampled CD-GW and canonical CD-GW. The fsCD-GW algorithm is always at least as fast or faster than the canonical CD-GW algorithm, making it generally applicable without any drawbacks. Starting from ten cadmium

TABLE II. Ionization energies of the open shell lanthanoid ions Ce^{3+} to Yb^{3+}, calculated at the evGW@PBE0 level of theory using canonical and frequency sampled (fs) contour deformation (CD) GW. All values in eV.

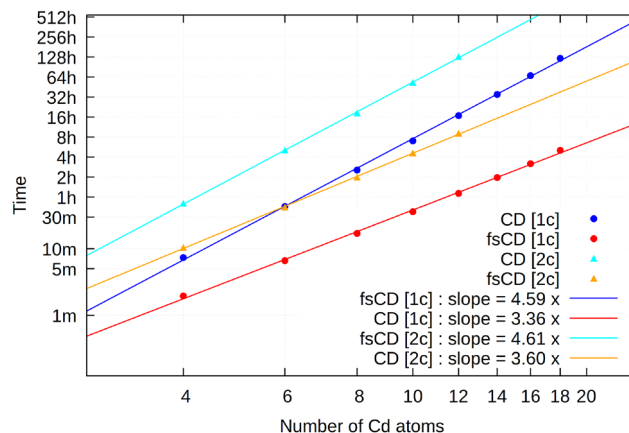| Ion	CD-evGW	fsCD-evGW	Reference
Ce^{3+}	36.270	36.265	36.91
Pr^{3+}	38.281	38.281	39.00
Nd^{3+}	40.151	40.151	40.60
Pm^{3+}	40.495	40.495	41.17
Sm^{3+}	40.842	40.842	41.64
Eu^{3+}	42.264	42.264	42.94
Gd^{3+}	43.712	43.712	44.44
Tb^{3+}	38.613	38.613	39.33
Dy^{3+}	40.710	40.707	41.23
Ho^{3+}	41.870	41.870	42.52
Er^{3+}	41.594	41.594	42.42
Tm^{3+}	41.724	41.724	42.41
Yb^{3+}	42.973	42.973	43.61

FIG. 2. Wall times for fsCD-G_0W_0 (red and orange) and CD-G_0W_0 (light and dark blue) for Cd clusters of varying sizes in one- (circles) and two-component (triangles) calculations for the lowest-lying orbital or spinor. Quasiparticle energies were obtained at the non-iterative G_0W_0 level, where the renormalization parameter was set to one. The scaling behavior or computational complexity is estimated from the slope of a linear regression using logarithmic scales for system size and CPU time and is shown in the graphs. The timings were recorded employing a Gauss–Legendre grid using 128 frequency points along the imaginary axis in the calculation of $I_\rho(\varepsilon_p)$. Deviations of the fsCD-G_0W_0 from the canonical CD-G_0W_0 algorithm were found to be $\sim 10^{-5}$ eV or lower in the above examples.

atoms, equaling 480 active electrons, 2c fsCD-G_0W_0 even becomes faster than 1c CD-G_0W_0, outlining the large gain in performance from reducing the scaling by an order of magnitude. Interestingly, for both the standard CD-G_0W_0 and the fsCD-G_0W_0 algorithm, the asymptotic limits of $\mathcal{O}(N^5)$ and $\mathcal{O}(N^4)$ are not yet reached, respectively. This can likely be attributed to the time limiting step, i.e., evaluating Eq. (10), not being fully dominating in the investigated systems. For the investigated cadmium clusters, we further note that the fsCD-G_0W_0 results are remarkably accurate. Deviations to the canonical algorithm are found to be 10^{-5} eV or lower for all cluster sizes. This outlines that the gain in efficiency does not affect the accuracy of the method, rendering fsCD-GW as an extremely favorable algorithm for non-valence states in general.

C. Core-electron ionization energies from the CORE65 set from the GW method

The CORE65 set of molecules is composed of mainly organic molecules, for which the 1s core-electron ionization energies have been assessed by Golze and co-workers in Ref. 72. In the latter work, only PBE and a hybrid PBEh variant with 45% HF exchange were investigated, with the latter being found to work reasonably well together with the G_0W_0 method. An ad hoc atom-dependent correction was added to the 1s orbital energies in Ref. 72 to account for relativistic effects. In this work, the X2C Hamiltonian in combination with the mSNSO approach is used to account for relativistic effects, therefore also entering the GKS density, and no further corrections are applied. The resulting statistical deviations of the obtained core ionization energies with respect to experimentally obtained values for the fsCD-G_0W_0 method are shown in Fig. 3. Due
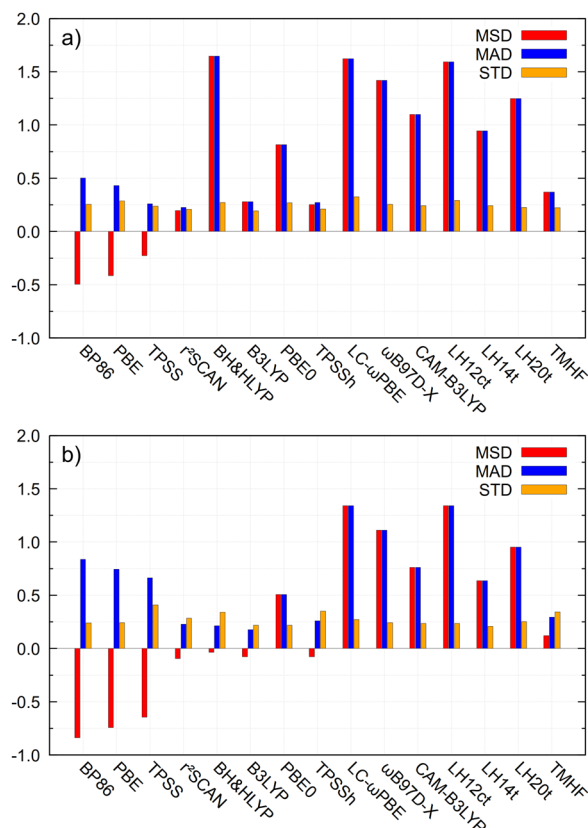
FIG. 3. Mean absolute deviation (MAD), mean signed deviation (MSD), and standard deviation (STD) for the fsCD-G_0W_0@DFT method using the (a) x2c-TZVPPall-2c and (b) x2c-QZVPPall-2c basis sets. All values in eV.

to the different treatment of relativistic effects, it is noted that the obtained results may differ from those previously obtained.[72]

For the all-electron x2c-TZVPPall-2c basis set, surprisingly, the pure DFAs and DFAs with a small amount of Hartree–Fock (HF) exchange yield lower deviations from the reference results when used together with the G_0W_0 when compared to DFAs with high amounts of HF exchange. This is in contrast to valence shell quasi-particle energies, where DFAs with a rather high amount of HF exchange and especially range-separated hybrid DFAs perform significantly better than pure DFAs or DFAs with a small amount of HF exchange.[100] BH & HLYP yields error comparable to those of range-separated hybrids, with PBE0 being in between those two classes. Range-separated hybrid DFAs with pre-determined parameters fail to provide good starting points for core ionization energies, which can simply be rationalized by the fact that core orbitals are well localized, with no general need for range separation arising for them. Furthermore, it has been shown that optimally tuned range-separated hybrid functionals can far exceed the performance of their pre-fitted counterparts, and we expect this to be the case also for core excitations.[101,102] It is, furthermore, notable that replacing the x2c-TZVPPall-2c basis set by the quadruple-ζ x2c-QZVPPall-2c basis set yields improved core ionization energies for generally all hybrid functionals but worsens the agreement of the pure density function-

als. Especially, BH & HLYP exhibits a large reduction in its overall deviation from experimental reference results as shown in Fig. 3(b), outlining that large basis sets are important when core ionization energies are tackled with DFAs that feature a high amount of HF exchange. The findings of Golze and co-workers that PBEh with 45% HF exchange also works well after a basis set extrapolation is, therefore, in good agreement with our data.[72] In combination with the x2c-QZVPPall-2c basis set, the hybrid DFAs B3LYP and TPSSh and the metaGGA r^{2}SCAN again provide excellent starting points.

For the class of local hybrids, TMHF excels for both basis sets, providing very good core-electron ionization energies. TMHF has high flexibility, allowing for incorporation of various amounts of non-local exchange depending on the density. This flexibility is key to an accurate description, allowing this functional to perform good performance. For fsCD-G_0W_0, it can, therefore, be concluded that r^{2}SCAN, B3LYP, TPSSh, and TMHF provide suitable starting points when combined with triple-ζ and quadruple-ζ size basis sets, hinting that only a moderate amount of HF exchange is important. Quadruple-ζ basis sets generally improve accuracy, especially for DFAs that incorporate larger amounts of HF exchange. As TMHF also provides accurate valence ionization energies when combined with the GW method,[28,89] it provides an excellent starting point for GW calculations in general.
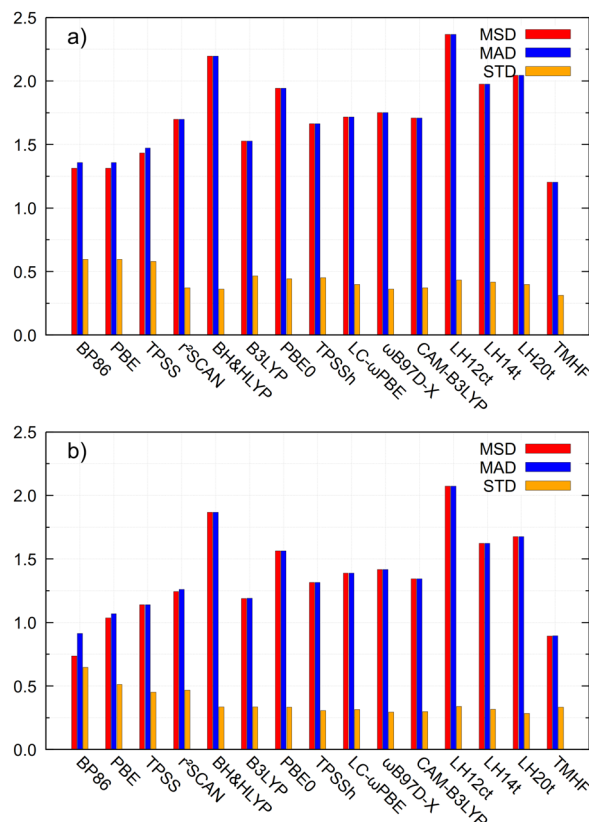

FIG. 4. Mean absolute deviation (MAD), mean signed deviation (MSD), and standard deviation (STD) for the fsCD-evGW@DFT method using the (a) x2c-TZVPPall-2c and (b) x2c-QZVPPall-2c basis sets. All values in eV.

15 August 2023 15:25:26

As shown in Fig. 4, partial self-consistency in the quasiparticle energies achieved through fsCD-evGW evens out most differences between the different GKS starting points. The only major outlier is the local hybrid TMHF, which remains significantly more precise compared to all other functionals when combined with fsCD-evGW. Using a larger quadruple-ζ basis set again significantly reduces all errors, with TMHF again providing the best performance by a good margin. Compared to fsCD-G_0W_0 results with the x2c-QZVPPall-2c basis set, the error of pure DFAs is significantly improved, but they still exhibit larger standard deviations than DFAs that include a low amount of HF exchange. Nevertheless, self-consistency in the quasiparticle energies fails to generally improve the accuracy of the GW method for core ionization energies. This is in line with earlier observations, finding errors of up to 1 eV for lower lying states.[103] Overall, the disappointing performance of evGW can be related to a worsened description of the density from the GKS reference in the vicinity of the nucleus. As evGW does not update the eigenvectors but is otherwise self-consistent, it is prone to amplify density errors. While this can be partly related to the density functional approximation itself, underscreening of the GW in the RPA approximation is another problem that becomes severe for core orbitals and could be corrected by the inclusion of vertex corrections.[103–105]

Compared to valence ionization energies, where hybrid and range-separated DFAs with high amounts of HF exchange perform best,[100] Figs. 3 and 4 give a qualitatively different picture. Pure DFAs and especially hybrid DFAs with moderate amounts of HF exchange perform rather well, while DFAs with high amounts of HF exchange perform comparably poor. *Ab initio* local hybrid DFAs as, for example, TMHF can bridge the gap and perform outstandingly well for both valence and core ionization energies.[89,106]

D. K- and L-edges of small inorganic molecules from the core–valence separated GW-BSE method

While the 1s states of the CORE65 test set are not affected by spin–orbit coupling, SOC effects become rather important for certain interesting K- and L-edges in molecular systems containing metal centers. Therefore, we chose to investigate 40 core excited states of eight transition metal molecules as shown in Fig. 5, where the inclusion of SOC is mandatory due to state splitting.
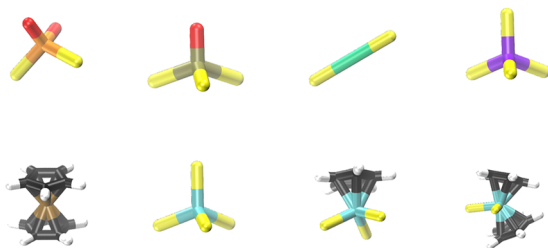

FIG. 5. Optimized geometries for the molecules in the test set considered in this section. The systems considered are from left to right, top to bottom, CrO_2Cl_2, $VOCl_3$, $PdCl_2$, $SiCl_4$, $FeCp_2$, $TiCl_4$, $TiCl_3Cp$, and $TiCl_2Cp_2$. The color scheme used here: oxygen (red), chloride (yellow), chromium (orange), vanadium (gray), palladium (green), silicon (violet), iron (brown), titanium (blue), carbon (black), and hydrogen (white).

The corresponding core excited states were calculated using the 2c CVS-BSE method outlined in Sec. III A, using PBE0 and a TMHF as GKS reference and quasiparticle energies from fsCD-G_0W_0 and fsCD-evGW. PBE0 is again chosen for its general availability and good performance, while TMHF is also compared due to being the single best density functional as outlined in Sec. V C. The resulting core excited states are compared to experimental values for which the statistical errors are provided in Table III. A detailed overview of all core excited states with the corresponding references can be found in the supplementary material. Overall, the results from the statistical evaluation presented in Table III are comparable to those obtained in Sec. V C, with fsCD-G_0W_0@TMHF being the best performing combination by a good margin. fsCD-G_0W_0@PBE0 performs significantly worse, especially for the high-energy K + L_1 edges. This is especially interesting given the fact that the initial starting GKS spinor energy of TMHF is assumed to be a worse approximation than the PBE0 one, as outlined in Ref. 15. As reference GKS determinant for a GW calculation, however, TMHF and other possible first principle local hybrid functionals are well suited, hinting at providing a reasonable description of the behavior of the electron density near the nucleus. The partially self-consistent fsCD-evGW variant again evens out the differences, with TMHF still performing superior to PBE0, but an overall reduced difference between both GKS references. The large maximum deviations found for all methods, but especially for PBE0 and fsCD-evGW@TMHF, can be traced back to the $TiCpCl_3$ complex, for which only fsCD-G_0W_0@TMHF

TABLE III. Mean signed deviation (MSD), mean absolute deviation (MAD), mean absolute percentwise deviation (MAPD), and standard deviation (STD) for the fsCD-G_0W_0-CVS-BSE and the fsCD-evGW-CVS-BSE methods. PBE0 and TMHF have been used as GKS references. MSD, MAD, and STD values in eV.

	PBE0		TMHF	
	G_0W_0	evGW	G_0W_0	evGW
K + L_1 edges				
MSD	2.92	4.47	1.01	4.00
MAD	3.35	5.28	2.05	4.37
MAPD	0.13	0.23	0.11	0.15
STD	3.21	5.92	2.11	5.02
Max.	10.27	16.87	3.31	11.68
$L_{2,3}$ edges				
MSD	0.02	1.10	0.07	0.72
MAD	0.92	1.11	0.92	0.83
MAPD	0.22	0.18	0.17	0.11
STD	1.21	1.10	1.53	1.49
Max.	4.03	4.81	6.28	6.81
Total				
MSD	0.75	1.94	0.31	1.54
MAD	1.53	2.15	1.20	1.72
MAPD	0.19	0.19	0.15	0.12
STD	2.25	3.34	1.71	3.09
Max.	10.27	16.87	6.28	11.68

yields reasonable values. The latter has a single outlier found for the $L_{2,3}$-edges of $PdCl_2$, which are, however, also present in all other combinations. Palladium $L_{2,3}$-edges are, therefore, by far the most troublesome in the investigated test set with deviations of up to 6 eV, which is an order of magnitude larger than the deviations found for other species. Subsequent testing hints that this error is a general failure of the GW-BSE method, as it is neither fixed by using the larger x2c-QZVPPall-2c basis set nor by dropping the CVS approximation as shown in Sec. V E. For palladium compounds, therefore, special care needs to be taken when those are tackled by the GW-BSE method, and an ad hoc shift parameter might be necessary. The remaining molecules, especially fsCD-G_0W_0, do a very good job predicting K- and L-edges, with mean absolute deviations of roughly 1 eV. The percentwise deviations outline that this is rather acceptable, given that core excitations are located in energy regimes of several 100 or even thousand eV. This is also confirmed when comparing our 2c fsCD-GW-BSE results to those of four-component (4c) damped response TD-DFT.[3] In Ref. 3, Konecny and co-workers have tested various DFAs for their reliability in obtaining core excitations. Table IV compares the 4c damped response TD-DFT results with the fsCD-GW-BSE results obtained in this work.

When inspecting the values obtained for $VOCl_3$ and CrO_2Cl_2, it is notable that fsCD-GW-BSE has a significantly reduced sensitivity to the chosen starting point when compared to TD-DFT. The latter can vary by as much as 20 eV for the same excitation, depending on the chosen DFA. This is also in agreement with the previous findings of the authors.[2] Contrary, fsCD-GW-BSE varies by a maximum of 2 eV for the core excitations listed in Table IV, reducing this variance by an order of magnitude. The overall agreement of fsCD-GW-BSE with experimental reference values is excellent, especially for the fsCD-G_0W_0@TMHF method, which was already found to provide the best accuracy overall. GW-BSE should, therefore, be preferred over TD-DFT for core excitations whenever possible.

E. Comparison of CVS-BSE and damped response BSE for core excitations

As noted by Herbst and Fransson in Ref. 107, the error of the CVS approximation compared to approaches employing the full excitation space can range from 0.02 to 0.20 eV for ADC(2). While this is significantly less than the statistical errors obtained for the BSE in Sec. V D, still one might want to take a closer look at the error introduced. While it has been shown that the error introduced by the CVS can partly be reversed,[108] the damped response formalism outlined in Sec. III B also provides a convenient alternative. As described in Sec. III A, there is no need to freeze valence orbitals to asses core excited states in the damped response for-

malism. Therefore, the CVS-BSE results of Sec. V D are compared to energy-integrated absorption cross sections σ obtained from the imaginary parts of the frequency-dependent polarizabilities,

$$\sigma(\omega) = \frac{4\pi\omega}{3c_{au}} \text{Im}[\text{Tr}(\boldsymbol{\alpha}(\omega))], \quad (33)$$

of the damped response BSE for the L_2-edge of $PdCl_2$, the $L_{2,3}$-edge of $TiCl_3Cp$, and the $L_{2,3}$-edge of $VOCl_3$, to provide an initial overview of the performance. The obtained results are shown in Fig. 6. $\text{Im}[\text{Tr}(\boldsymbol{\alpha}(\omega))]$ in Eq. (33) refers to the imaginary part of the frequency-dependent polarizability at a frequency ω, and c_{au} is the speed of light in atomic units. For the L_2-edge of $PdCl_2$, as shown in Fig. 6(a), there is barely any difference between CVS-BSE and the full damped response BSE. Electronic positions are near perfect, and only very slight deviations in the absorption cross section can be seen, far below the error bars of standard GW-BSE. This outlines that for isolated bands, CVS-BSE might be a near ideal approximation to the full BSE response. For $TiCpCl_3$ and $VOCl_2$, shown in Figs. 6(b) and 6(d), again excellent agreement between the CVS-BSE and damped response BSE is observed. Both, peak positions and absorption cross sections are in close agreement, with only insignificant differences between CVS-BSE and damped response BSE. For the more complicated L-edge of CrO_2Cl_2, matters are different as can be seen in Fig. 6(c). Some bands are perfectly reproduced, while for other band, the position is well reproduced, but the absorption cross section is severely underestimated. For example, the CVS-BSE approach fails to reproduce the band slightly below 577 eV and the bands at ~578, 581.5, 583, 585.5, and 587 eV. As outlined by Konecny and co-workers in the framework of TD-DFT, these states can be identified as intruder states, arising from excitations of valence spinors to higher lying virtual pseudo-continuum states, artificially mixing into the core excitation spectrum.[3] As outlined in Sec. III B, this problem only plagues the damped response BSE formalism but is effectively suppressed by the CVS approximation. Similar to TD-DFT, a possible solution would be to introduce the CVS approximation in the damped response formalism, again projecting out the corresponding ill-behaved excitations. While this would be unfeasible for the comparison made in this work, it can be a valid tactic in regions with a high density of excited states that are otherwise inaccessible and plagued by these intruder states. Another solution is to simply zero out all matrix elements of the dipole operator in Eq. (30) that do not belong to the atomic shell of interest.[3,109] The latter approach allows us to still introduce core–valence correlation to some extend and has been successfully applied in real-time TD-DFT simulation.[109]

TABLE IV. Comparison of the $L_{2,3}$-edges of the metal centers in $VOCl_3$ and CrO_2Cl_2. DFT result taken from Ref. 3. Experimental results taken from Ref. 90. All values in eV.

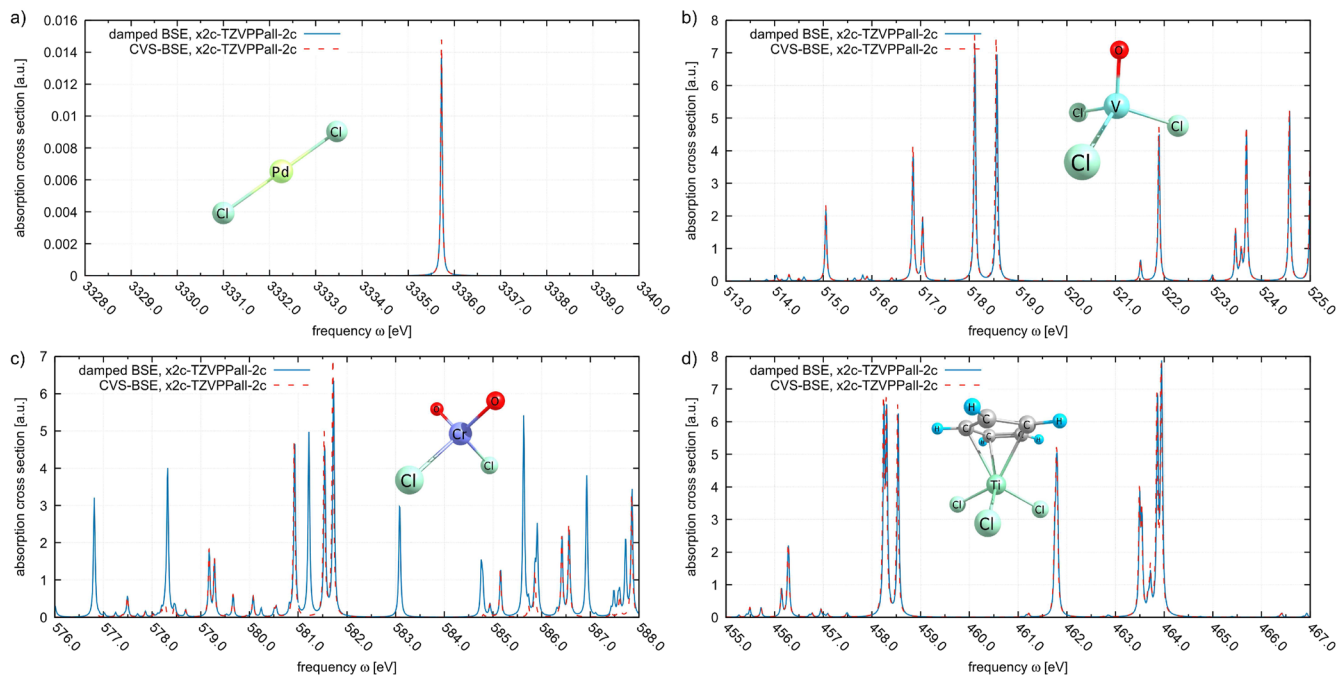| Molecule	Edge	PBE	PBE0 25%	PBE0 40%	CAM-B3LYP	B3LYP	G_0W_0-BSE PBE0	G_0W_0-BSE TMHF	evGW-BSE PBE0	evGW-BSE TMHF	Exp.
$VOCl_3$	L_3	499.2	507.5	512.1	506.0	506.0	516.8	516.6	518.0	516.8	516.9
	L_2	505.9	514.2	518.9	512.8	512.8	521.8	523.5	523.3	523.5	523.2
CrO_2Cl_2	L_3	562.2	571.4	576.6	569.8	569.8	581.6	580.0	582.5	579.9	578.0
	L_2	570.8	579.5	584.8	577.9	577.9	586.8	586.9	587.2	587.4	587.2

FIG. 6. Damped response BSE (blue solid lines) and CVS-BSE XAS spectra (red dashed lines) comparing the energy-integrated absorption cross section of (a) the Pd L_2-edge, (b) the $VOCl_3$ $L_{2,3}$-edges, (c) the CrO_2Cl_2 $L_{2,3}$-edges, and (d) the $TiCpCl_3$ $L_{2,3}$-edges. All spectra were calculated at the fsCD-G_0W_0@TMHF level of theory. A damping parameter of 0.02 eV was used for damped response BSE. CVS-BSE spectra were broadened accordingly with Lorentzians. Absorption cross section is given in atomic units (= bohrs^2 hartree), frequency in eV.

VI. CONCLUSION

In this work, a relativistic frequency-sampled contour deformation based GW approach, labeled fsCD-GW, was outlined and implemented. fsCD-GW is an accurate yet efficient method to assess the quasiparticle energies of orbitals and spinors far away from the Fermi level, while fully taking spin–orbit coupling into account if needed. Computationally, fsCD-GW reduces the scaling by an order of magnitude when compared to canonical CD-GW and by two orders of magnitude if compared with spectral algorithms.[70,110] This computational advantage is accompanied by an intrinsically high accuracy, with results practically identical to those of the canonical algorithms. This high accuracy can even be maintained for the core and valence states of open-shell relativistic lanthanoid ions, which are among the electronically most complicated systems tackled by the GW approximation to date. Using fsCD-GW, the performance of various density functional approximations as reference GKS determinants for the GW approximation has been tested. Contrary to valence excitations, DFAs with a low amount of HF exchange, as well as the local hybrid functional TMHF, were found to be best suited to perform GW calculations for core ionized states. Furthermore, the fsCD-GW-BSE method was used to assess the core excited states of small molecules with metal centers. The core–valence separation approximation for the BSE was shown to yield reliable excitation energies and absorption cross sections for these core excited states. The combined fsCD-GW plus damped response BSE approach will also be a highly valuable tool

for valence spectra with a very high density of states, as, for example, in nanoparticles.[111] Furthermore, recent developments in multiscale modeling of optical materials also rely on a similar approach,[112,113] and thus, the efficient fsCD-GW-BSE approach will make *ab initio* many-body multiscale simulations feasible with tools other than time-dependent DFT.

SUPPLEMENTARY MATERIAL

See the supplementary material for a discussion and graphical representation of the correlation part of the self-energy of the Nd^{3+} ion, the correlation part of the self-energy of the water molecule, individual core ionization energies of the CORE65 test set for all 15 tested density functional approximation, the individual values of the core excited states calculated for the eight small molecules in Sec. V D, and the corresponding optimized geometries of these eight molecules as ASCII coordinate files.

ACKNOWLEDGMENTS

AUTHOR DECLARATIONS
Conflict of Interest

The authors have no conflicts to disclose.

Author Contributions

Max Kehry: Conceptualization (lead); Data curation (lead); Investigation (lead); Methodology (lead); Software (lead); Validation (lead); Writing – original draft (supporting); Writing – review & editing (supporting). **Wim Klopper**: Conceptualization (supporting); Supervision (lead); Writing – review & editing (supporting). **Christof Holzer**: Conceptualization (supporting); Data curation (supporting); Investigation (supporting); Methodology (supporting); Software (supporting); Validation (supporting); Writing – original draft (lead); Writing – review & editing (lead).

DATA AVAILABILITY

The data that support the findings of this study are available within the article and its supplementary material.

REFERENCES

[1] T. Vitova, P. W. Roesky, and S. Dehnen, Commun. Chem. **5**, 12 (2022).

[2] M. Kehry, Y. J. Franzke, C. Holzer, and W. Klopper, Mol. Phys. **118**, e1755064 (2020).

[3] L. Konecny, J. Vicha, S. Komorovsky, K. Ruud, and M. Repisky, Inorg. Chem. **61**, 830 (2022).

[4] M. Stener, G. Fronzoni, and M. de Simone, Chem. Phys. Lett. **373**, 115 (2003).

[5] K. Lopata, B. E. Van Kuiken, M. Khalil, and N. Govind, J. Chem. Theory Comput. **8**, 3284 (2012).

[6] T. Fransson, I. E. Brumboiu, M. L. Vidal, P. Norman, S. Coriani, and A. Dreuw, J. Chem. Theory Comput. **17**, 1618 (2021).

[7] P. Verma and D. G. Truhlar, Trends Chem. **2**, 302 (2020) part of special issue: Laying Groundwork for the Future.

[8] N. A. Besley, Wiley Interdiscip. Rev.: Comput. Mol. Sci. **11**, e1527 (2021).

[9] Y. Imamura, T. Otsuka, and H. Nakai, J. Comput. Chem. **28**, 2067 (2007).

[10] D. Mester and M. Kállay, J. Chem. Theory Comput. **19**, 1310 (2023).

[11] Y. Yao, D. Golze, P. Rinke, V. Blum, and Y. Kanai, J. Chem. Theory Comput. **18**, 1569 (2022).

[12] D. Golze, J. Wilhelm, M. J. van Setten, and P. Rinke, J. Chem. Theory Comput. **14**, 4856 (2018).

[13] G. Fronzoni, M. Stener, P. Decleva, F. Wang, T. Ziegler, E. van Lenthe, and E. Baerends, Chem. Phys. Lett. **416**, 56 (2005).

[14] C. Holzer and W. Klopper, J. Chem. Phys. **150**, 204116 (2019).

[15] C. Holzer, J. Chem. Theory Comput. **19**, 3131–3145 (2023).

[16] G. Strinati, H. J. Mattausch, and W. Hanke, Phys. Rev. Lett. **45**, 290 (1980).

[17] A. Fleszar and W. Hanke, Phys. Rev. B **56**, 10228 (1997).

[18] R. W. Godby, M. Schlüter, and L. J. Sham, Phys. Rev. B **37**, 10159 (1988).

[19] I. Duchemin and X. Blase, J. Chem. Theory Comput. **16**, 1742 (2020).

[20] D. Foerster, P. Koval, and D. Sánchez-Portal, J. Chem. Phys. **135**, 074105 (2011).

[21] X. Ren, P. Rinke, C. Joas, and M. Scheffler, J. Mater. Sci. **47**, 7447 (2012).

[22] P. Liu, M. Kaltak, J. c. v. Klimeš, and G. Kresse, Phys. Rev. B **94**, 165109 (2016).

[23] M. Govoni and G. Galli, J. Chem. Theory Comput. **11**, 2680 (2015).

[24] P. Scherpelz, M. Govoni, I. Hamada, and G. Galli, J. Chem. Theory Comput. **12**, 3523 (2016).

[25] V. Vlček, E. Rabani, D. Neuhauser, and R. Baer, J. Chem. Theory Comput. **13**, 4997 (2017).

[26] I. Duchemin and X. Blase, J. Chem. Theory Comput. **17**, 2383 (2021).

[27] A. Förster and L. Visscher, Front. Chem. **9**, 736591 (2021).

[28] L. Monzel, C. Holzer, and W. Klopper, J. Chem. Phys. **158**, 144102 (2023).

[29] J. M. Kasper, A. J. Jenkins, S. Sun, and X. Li, J. Chem. Phys. **153**, 090903 (2020).

[30] H. F. Schurkus and C. Ochsenfeld, J. Chem. Phys. **144**, 031101 (2016).

[31] D. Graf, M. Beuerle, H. F. Schurkus, A. Luenser, G. Savasci, and C. Ochsenfeld, J. Chem. Theory Comput. **14**, 2505 (2018).

[32] J. Wilhelm, D. Golze, L. Talirz, J. Hutter, and C. A. Pignedoli, J. Phys. Chem. Lett. **9**, 306 (2018).

[33] I. Duchemin and X. Blase, J. Chem. Phys. **150**, 174120 (2019).

[34] A. Förster and L. Visscher, J. Chem. Theory Comput. **16**, 7381 (2020).

[35] J. Wilhelm, P. Seewald, and D. Golze, J. Chem. Theory Comput. **17**, 1662 (2021).

[36] M. J. van Setten, F. Weigend, and F. Evers, J. Chem. Theory Comput. **9**, 232 (2013).

[37] F. Kaplan, F. Weigend, F. Evers, and M. J. van Setten, J. Chem. Theory Comput. **11**, 5152 (2015).

[38] L. Hedin, Nucl. Instrum. **308**, 169 (1991).

[39] L. Hedin, Phys. Rev. **139**, A796 (1965).

[40] M. L. Tiago and J. R. Chelikowsky, Phys. Rev. B **73**, 205334 (2006).

[41] J. Wilhelm, M. Del Ben, and J. Hutter, J. Chem. Theory Comput. **12**, 3623 (2016).

[42] M. Kühn and F. Weigend, J. Chem. Theory Comput. **11**, 969 (2015).

[43] N. Pueyo Bellafont, P. S. Bagus, and F. Illas, J. Chem. Phys. **142**, 214102 (2015).

[44] A. C. Antoulas and B. D. Q. Anderson, IMA J. Math. Control. Inf. **3**, 61 (1986).

[45] Y. Nakatsukasa, O. Sète, and L. N. Trefethen, SIAM J. Sci. Comput. **40**, A1494 (2018).

[46] S. Coriani and H. Koch, J. Chem. Phys. **143**, 181103 (2015).

[47] J. Liu, D. Matthews, S. Coriani, and L. Cheng, J. Chem. Theory Comput. **15**, 1642 (2019).

[48] I. Seidu, S. P. Neville, M. Kleinschmidt, A. Heil, C. M. Marian, and M. S. Schuurman, J. Chem. Phys. **151**, 144104 (2019).

[49] R. Faber and S. Coriani, Phys. Chem. Chem. Phys. **22**, 2642 (2020).

[50] P. Norman and A. Dreuw, Chem. Rev. **118**, 7208 (2018).

[51] B. N. C. Tenorio, T. Moitra, M. A. C. Nascimento, A. B. Rocha, and S. Coriani, J. Chem. Phys. **150**, 224104 (2019).

[52] K. Krause and W. Klopper, J. Comput. Chem. **38**, 383 (2017).

[53] X. Blase, I. Duchemin, and D. Jacquemin, Chem. Soc. Rev. **47**, 1022 (2018).

[54] C. Holzer and W. Klopper, J. Chem. Phys. **149**, 101101 (2018).

[55] E. Monino and P.-F. Loos, J. Chem. Theory Comput. **17**, 2852 (2021).

[56] U. Ekström, P. Norman, V. Carravetta, and H. Ågren, Phys. Rev. Lett. **97**, 143001 (2006).

[57] S. M. Parker, S. Roy, and F. Furche, J. Chem. Phys. **145**, 134105 (2016).

[58] C. Holzer and W. Klopper, J. Chem. Phys. **147**, 181101 (2017).

[59] Y. J. Franzke, C. Holzer, and F. Mack, J. Chem. Theory Comput. **18**, 1030 (2022).

[60] S. G. Balasubramani, G. P. Chen, S. Coriani, M. Diedenhofen, M. S. Frank, Y. J. Franzke, F. Furche, R. Grotjahn, M. E. Harding, C. Hättig, A. Hellweg, B. Helmich-Paris, C. Holzer, U. Huniar, M. Kaupp, A. Marefat Khah, S. Karbalaei Khani, T. Müller, F. Mack, B. D. Nguyen, S. M. Parker, E. Perlt, D. Rappoport, K. Reiter, S. Roy, M. Rückert, G. Schmitz, M. Sierka, E. Tapavicza, D. P. Tew, C. van Wüllen, V. K. Voora, F. Weigend, A. Wodyński, and J. M. Yu, J. Chem. Phys. **152**, 184107 (2020).

[61] Y. J. Franzke, C. Holzer, J. H. Andersen, T. Begušić, F. Bruder, S. Coriani, F. Della Sala, E. Fabiano, D. A. Fedotov, S. Fürst, S. Gillhuber, R. Grotjahn, M. Kaupp, M. Krstić, F. Mack, S. Majumdar, B. D. Nguyen, S. M. Parker, F. Pauly, A. Pausch, E. Perlt, G. S. Phun, A. Rajabi, D. Rappoport, B. Samal, T. Schrader, M. Sharma, E. Tapavicza, R. S. Treß, V. Voora, A. Wodyński, J. M. Yu, B. Zerulla, F. Furche, C. Hättig, M. Sierka, D. P. Tew, and F. Weigend, J. Chem. Theory Comput. (published online) (2023).

[62] C. Holzer, J. Chem. Phys. **153**, 184115 (2020).

[63] OpenMP Architecture Review Boards, "OpenMP API shared-memory parallel programming," https://www.openmp.org, retrieved December 4, 2020.

[64] C. Holzer and Y. J. Franzke, OpenMP version of ridft, rdgrad, and egrad with contributions to mpshift, dscf, and grad; improved OpenMP version of aoforce and escf, released with TURBOMOLE V7.4 and further improved in TURBOMOLE V7.5.

[65] P. Pollak and F. Weigend, J. Chem. Theory Comput. **13**, 3696 (2017).

[66] Y. J. Franzke, L. Spiske, P. Pollak, and F. Weigend, J. Chem. Theory Comput. **16**, 5658 (2020).

[67] O. Treutler and R. Ahlrichs, J. Chem. Phys. **102**, 346 (1995).

[68] Y. J. Franzke, N. Middendorf, and F. Weigend, J. Chem. Phys. **148**, 104410 (2018).

[69] L. Visscher and K. G. Dyall, At. Data Nucl. Data Tables **67**, 207 (1997).

[70] C. Holzer, A. M. Teale, F. Hampe, S. Stopkowicz, T. Helgaker, and W. Klopper, J. Chem. Phys. **150**, 214112 (2019).

[71] S. Kohaut and M. Springborg, Phys. Chem. Chem. Phys. **18**, 28524 (2016).

[72] D. Golze, L. Keller, and P. Rinke, J. Phys. Chem. Lett. **11**, 1840 (2020).

[73] J. P. Perdew, Phys. Rev. B **33**, 8822 (1986).

[74] A. D. Becke, Phys. Rev. A **38**, 3098 (1988).

[75] J. P. Perdew, K. Burke, and M. Ernzerhof, Phys. Rev. Lett. **77**, 3865 (1996).

[76] J. Tao, J. P. Perdew, V. N. Staroverov, and G. E. Scuseria, Phys. Rev. Lett. **91**, 146401 (2003).

[77] J. Sun, A. Ruzsinszky, and J. P. Perdew, Phys. Rev. Lett. **115**, 036402 (2015).

[78] J. W. Furness, A. D. Kaplan, J. Ning, J. P. Perdew, and J. Sun, J. Phys. Chem. Lett. **11**, 8208 (2020).

[79] C. Lee, W. Yang, and R. G. Parr, Phys. Rev. B **37**, 785 (1988).

[80] A. D. Becke, J. Chem. Phys. **98**, 1372 (1993).

[81] C. Adamo and V. Barone, J. Chem. Phys. **110**, 6158 (1999).

[82] V. N. Staroverov, G. E. Scuseria, J. Tao, and J. P. Perdew, J. Chem. Phys. **119**, 12129 (2003).

[83] T. Yanai, D. P. Tew, and N. C. Handy, Chem. Phys. Lett. **393**, 51 (2004).

[84] J.-D. Chai and M. Head-Gordon, Phys. Chem. Chem. Phys. **10**, 6615 (2008).

[85] O. A. Vydrov and G. E. Scuseria, J. Chem. Phys. **125**, 234109 (2006).

[86] A. V. Arbuznikov and M. Kaupp, J. Chem. Phys. **136**, 014111 (2012).

[87] A. V. Arbuznikov and M. Kaupp, J. Chem. Phys. **141**, 204101 (2014).

[88] M. Haasler, T. M. Maier, R. Grotjahn, S. Gückel, A. V. Arbuznikov, and M. Kaupp, J. Chem. Theory Comput. **16**, 5645 (2020).

[89] C. Holzer and Y. J. Franzke, J. Chem. Phys. **157**, 034108 (2022).

[90] G. Fronzoni, M. Stener, P. Decleva, M. d. Simone, M. Coreno, P. Franceschi, C. Furlani, and K. C. Prince, J. Phys. Chem. A **113**, 2914 (2009).

[91] T. Sham, Chem. Phys. Lett. **101**, 567 (1983).

[92] J. Bozek, K. Tan, G. Bancroft, and J. Tse, Chem. Phys. Lett. **138**, 33 (1987).

[93] I. Ismail, R. Guillemin, T. Marchenko, O. Travnikova, J. M. Ablett, J.-P. Rueff, M.-N. Piancastelli, M. Simon, and L. Journel, Rev. Sci. Instrum. **89**, 063107 (2018).

[94] K. Godehusen, T. Richter, P. Zimmermann, and P. Wernet, J. Phys. Chem. A **121**, 66 (2017).

[95] S. DeBeer George, P. Brant, and E. I. Solomon, J. Am. Chem. Soc. **127**, 667 (2005).

[96] A. Wen and A. Hitchcock, Can. J. Chem. **71**, 1632 (1993).

[97] J. C. Boettger, Phys. Rev. B **62**, 7809 (2000).

[98] M. Filatov, W. Zou, and D. Cremer, J. Chem. Phys. **139**, 014106 (2013).

[99] W. Zou, M. Filatov, and D. Cremer, J. Chem. Phys. **142**, 214106 (2015).

[100] F. Bruneval and M. A. L. Marques, J. Chem. Theory Comput. **9**, 324 (2013).

[101] C. A. McKeon, S. M. Hamed, F. Bruneval, and J. B. Neaton, J. Chem. Phys. **157**, 074103 (2022).

[102] S. E. Gant, J. B. Haber, M. R. Filip, F. Sagredo, D. Wing, G. Ohad, L. Kronik, and J. B. Neaton, Phys. Rev. Mater. **6**, 053802 (2022).

[103] D. Golze, M. Dvorak, and P. Rinke, Front. Chem. **7**, 377 (2019).

[104] F. Caruso, M. Dauth, M. J. van Setten, and P. Rinke, J. Chem. Theory Comput. **12**, 5076 (2016).

[105] M. Grumet, P. Liu, M. Kaltak, J. c. v. Klimeš, and G. Kresse, Phys. Rev. B **98**, 155143 (2018).

[106] C. Holzer, Y. J. Franzke, and M. Kehry, J. Chem. Theory Comput. **17**, 2928 (2021).

[107] M. F. Herbst and T. Fransson, J. Chem. Phys. **153**, 054114 (2020).

[108] J. H. Andersen, K. D. Nanda, A. I. Krylov, and S. Coriani, J. Chem. Theory Comput. **18**, 6189 (2022).

[109] M. Kadek, L. Konecny, B. Gao, M. Repisky, and K. Ruud, Phys. Chem. Chem. Phys. **17**, 22566 (2015).

[110] C. Holzer, A. Pausch, and W. Klopper, Front. Chem. **9**, 746162 (2021).

[111] M. M. Müller, N. Perdana, C. Rockstuhl, and C. Holzer, J. Chem. Phys. **156**, 094103 (2022).

[112] B. Zerulla, M. Krstić, D. Beutel, C. Holzer, C. Wöll, C. Rockstuhl, and I. Fernandez-Corbaton, Adv. Mater. **34**, 2200350 (2022).

[113] B. Zerulla, C. Li, D. Beutel, S. Oßwald, C. Holzer, J. Bürck, S. Bräse, C. Wöll, I. Fernandez-Corbaton, L. Heinke, C. Rockstuhl, and M. Krstić, Adv. Funct. Mater. (published online) (2023).

15 August 2023 15:25:26